

Learning Homeomorphic Image Registration via Conformal-Invariant Hyperelastic Regularisation

Jing Zou^{a,b,1}, Noémie Debroux^c, Lihao Liu^b, Jing Qin^{a,*}, Carola-Bibiane Schönlieb^b, Angelica I Aviles-Rivero^b

^a*Center for Smart Health, School of Nursing, The Hong Kong Polytechnic University, HKSAR, China*

^b*Department of Applied Mathematics and Theoretical Physics, University of Cambridge, Cambridge, UK*

^c*Université Clermont Auvergne, France*

Abstract

Deformable image registration is a fundamental task in medical image analysis and plays a crucial role in a wide range of clinical applications. Recently, deep learning-based approaches have been widely studied for deformable medical image registration and achieved promising results. However, existing deep learning image registration techniques do not theoretically guarantee topology-preserving transformations. This is a key property to preserve anatomical structures and achieve plausible transformations that can be used in real clinical settings. We propose a novel framework for deformable image registration. Firstly, we introduce a novel regulariser based on conformal-invariant properties in a nonlinear elasticity setting. Our regulariser enforces the deformation field to be smooth, invertible and orientation-preserving. More importantly, we strictly guarantee topology preservation yielding to a clinical meaningful registration. Secondly, we boost the performance of our regulariser through coordinate MLPs, where one can view the to-be-registered images as continuously differentiable entities. We demonstrate, through numerical and visual experiments, that our framework is able to outperform current techniques for image registration.

Keywords: Homeomorphic Image Registration, Lung CT, Conformal Invariant Hyperelastic Regularisation

1. Introduction

Deformable image registration (DIR) is a crucial tool in modern healthcare, allowing physicians to compare and combine information from multiple images of the same patient or different patients. It is a fundamental task in medical images analysis and plays a key role in various clinical applications including image-guided interventions (Tam et al., 2016), radiotherapy (Krilavicius et al., 2016; Brock et al., 2017) diagnosis (Tekchandani et al., 2022), and treatment planning (Krilavicius et al., 2016).

DIR aims to align two or more images by optimising a non-linear voxel-wise deformation mapping between the given target and source images. Traditional methods treat DIR as a pair-wise optimisation problem, which relies on specific modelling assumptions. As a result, flexibility is limited, and it is difficult to handle complex and unpredictable deformations. Furthermore, the selection of an appropriate model, that accurately

represents the deformation, can be challenging. In addition, such iterative optimisation process is often time-consuming, which limits their applicability in real-time clinical scenarios.

Learning-based approaches have proliferated and have been widely studied for DIR and achieved promising results e.g. (Çiçek et al., 2016; Heinrich, 2019; Long et al., 2015; Ronneberger et al., 2015; Liu et al., 2019a; Zou et al., 2022). Following this research line, several techniques and strategies have been proposed to improve registration performance. For example, cascaded networks (Zhao et al., 2019a), pyramid coarse-to-fine networks (Mok and Chung, 2020) or joint models (Liu et al., 2021). However, the improvements are limited due to two main challenges. Firstly, existing models assume to have, for the training stage, a large and well-represented dataset. However, in medical domain, acquiring such dataset is challenging. Additionally, even with a large dataset, the representations learned from training data cannot capture the optimal complex deformations for all image pairs. Secondly, current learning-based methods cannot theoretically and strictly guarantee diffeomorphism of the deformation field. Although

* Corresponding author: harry.qin@polyu.edu.hk

¹ Work done during a visiting in Cambridge

L^2 regularisation (Balakrishnan et al., 2019; Hering et al., 2021), cycle consistency constraint (Kim et al., 2021) and inverse consistency constraint (Zhu and Lu, 2022; Liu et al., 2022) are utilised to improve the quality of deformation fields, these frameworks strictly cannot theoretically guarantee diffeomorphic transformations—this is reflected in reporting negative values in the Jacobian determinant.

To handle the aforementioned challenges, optimising pair-wise transformations has been explored from the variational and learning perspectives. This set of techniques mitigates the need of having a large dataset. A crucial factor, for any type of image registration methods, is the regulariser used to enforce plausible transformations. For example, the community largely has used Laplacian constraints, incompressibility constraints, and fluid-like regularisers (Passieux and Périé, 2012; Christensen et al., 1996; Mansi et al., 2011). However, these regularisers fail to handle large deformations or do not capture the characteristics of the target tissues. Perhaps hyperelastic regularisation (Veress et al., 2005; Phatak et al., 2009; Burger et al., 2013) is the most widely used constraint in the medical domain; as this principle matches with the characteristics of biological tissues. Learning-based methods for pair-wise registration have also used such types of regularisers. For example, the work of that (Wolterink et al., 2022) used the existing hyperelastic regulariser of (Burger et al., 2013). A weak constraint has been imposed on the Jacobian determinant in (Han et al., 2023). In contrast to those works that use existing regularisers. In this work, we focus on proposing a novel regulariser that is more flexible and can provide theoretical guarantees.

We summarise the contributions as follows:

- We propose a novel pair-wise image registration framework that eliminates the need for pre-training or prior affine registration.
- The key contribution of this paper is that we introduce a novel conformal-invariant regulariser. The proposed regulariser unifies the hyperelasticity with conformal and Beltrami-based approaches. It enables simultaneous control of changes in length, area, and volume and of distortion with conformal mappings, as well as smoothness of deformations. Most importantly, *our regulariser yields to homeomorphic transformations enforcing plausible transformations and theoretical guarantees*.
- We introduce a learned image deformation mapping that is driven by our novel regulariser via

coordinate MLP, and the learning process is resolution-independent, offering more flexibility.

- We demonstrate, through extensive experimental results, that our proposed framework yields to better performance than existing implicit and explicit regularisers.

2. Related Works

In this section, we thoroughly examine the existing literature and highlight the distinctive aspects of our work in comparison.

2.1. Traditional Methods

Over the past few decades, the field of image registration has primarily focused on traditional methods, leading to the development of toolboxes such as Elastix (Klein et al., 2009) and ANTs (Avants et al., 2009). These methods typically involve defining a transformation model, an optimisation function, and a similarity metric, followed by an iterative parameter optimisation process to find the optimal transformation. Various mathematical models have been utilized in these methods, including elastic-type models (Bajcsy and Kovačič, 1989), free-form deformation models based on cubic B-splines (Rueckert et al., 1999), statistical parametric mapping (Ashburner and Friston, 2000), and Demons-based approaches (Pennec et al., 1999). In order to ensure smoother and invertible deformation fields, diffeomorphic transformations have gained significant attention in the past decades (Oliveira and Tavares, 2014). Prominent examples of diffeomorphic transformation methods include Large deformation diffeomorphic metric mapping (LDDMM)(Beg et al., 2005; Cao et al., 2005; Glaunès et al., 2008), Symmetric Normalization (SyN)(Rogelj and Kovačič, 2006; Beg and Khan, 2007; Avants et al., 2008) (integrated into ANTs), and diffeomorphic Demons (Vercauteren et al., 2009). Despite their achievements, these methods are computationally intensive due to their reliance on iterative optimisation strategies. In addition, selecting an appropriate transformation model that accurately captures the deformations between input image pairs is still challenging.

2.2. Learning-based Methods

In learning-based methods, the deformation mapping from the source image to the target image is typically parameterised via deep networks, and the mapping is learned from lots of training image pairs. The main

advantage of learning-based methods is the remarkable speed in the inference phase once the training is complete.

Supervised learning methods usually rely on ground truth deformation fields, which are either obtained from traditional methods (Yang et al., 2017; Fan et al., 2019) or synthesized through manual deformable transformation (Sokooti et al., 2017, 2019). However, there are challenges associated with obtaining ground truth deformation fields. On one hand, generating real deformation fields can be time-consuming and computationally expensive. On the other hand, using pseudo ground-truth deformation fields that obtained through manual deformable transformations may not accurately represent the true distribution of misalignments in real-world scenarios.

To handle the challenges, researchers have turned to unsupervised methods, whose training relies on image-wise similarities rather than the ground truth deformation fields. The popular VoxelMorph (Balakrishnan et al., 2019) is based on Unet for deformable brain MR image registration. With only paired images as input, VoxelMorph efficiently predicts the corresponding deformation field, and the network is updated by minimizing the intensity-based discrepancy between the warped and the target images. Besides, other strategies are proposed to improve the performance of learning-based registration methods. For example, cascaded networks (Zhao et al., 2019a,b), multi-stage pyramid network (De Vos et al., 2019; Mok and Chung, 2020), and weak supervisions (Xu and Niethammer, 2019; Hering et al., 2021). In cascaded networks, the source image is progressively warped by the deformation field from each cascade network, finally aligned to the target image. The final deformation field is the composition of all fields from these cascaded networks. In multi-stage pyramid network, the deformation field is learned in a coarse-to-fine manner, where the registration is performed at multiple scales of image pyramids. For weak supervisions, the segmentation masks or the anatomical landmarks are utilized to guide the learning.

Although these methods have demonstrated improvement of the registration performance, there still exist challenges for learning-based methods. Firstly, the training of these networks usually requires a large dataset. However, acquiring a well-represented and sufficiently large dataset in the medical domain is challenging. Secondly, they can not theoretically guarantee the diffeomorphism of the learned deformation field.

2.3. Regularisations in Registration

In deformable medical image registration, anatomical structures often exhibit local and non-rigid variations. Achieving accurate registration necessitates a deformation field capable of capturing these variations at a high resolution with a high degree of freedom. The most challenging part of such registration is to ensure that the estimated deformation field between images is smooth and realistic, while avoiding overfitting due to the high degree of freedom. The key to a successful registration is the choice of the regularisation as it determines the types of transformations that the model can generate.

In traditional registration methods, many regularisations are proposed and they are commonly model-dependent. In the elastic model, the first-order derivatives or the second-order derivatives of the deformation field are penalised to ensure the smoothness (Modersitzki, 2003). Regularisation for the B-spline model is performed by applying constraints on the displacements of the B-spline control points (Rueckert et al., 1999). For fluid models, the regularisation is employed by penalising spatial derivatives of the velocity fields (Vialard et al., 2012). Additionally, laplacian constraints, incompressibility constraints, and fluid-like regularisers (Passieux and Périé, 2012; Christensen et al., 1996; Mansi et al., 2011) are proposed for specific registration tasks.

Many learning-based registration methods employ a simple and generic regularization, which takes the form of a penalty on the first-order derivative of the deformation field (Balakrishnan et al., 2018, 2019; Hering et al., 2021; Zhao et al., 2019a). The performance is limited as it assumes uniform smoothness properties irrespective of image content and allowable deformations. Furthermore, some networks utilised cycle consistency constraint (Kim et al., 2019, 2021) and inverse consistency constraint (Zhu and Lu, 2022; Liu et al., 2022) to improve the quality of the deformation field. However, these constraints are performed in a bi-directional manner, which introduces additional computational complexity. Moreover, they can not theoretically guarantee plausible transformations.

3. Methodology

This section describes our novel image registration framework. It contains two key parts: i) the introduction and motivation of our new conformal-invariant hyperelastic-based regulariser to impose a physically relevant nature on the deformation, and ii) the details

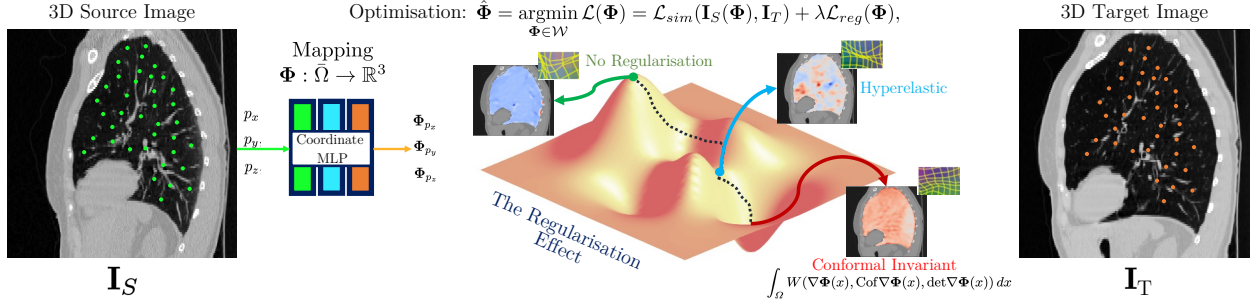


Figure 1: Our proposed workflow framework. We seek to optimise, through a coordinate MLP, the mapping Φ to align the coordinates between the source and target images. Our highlight is a new regulariser, whose effect is illustrated in the middle part. Our proposed conformal-invariant hyperelastic regulariser enforces volume preservation, controls changes in length and area, and ensures smoothness of deformation yielding to a better optimisation outcome.

of our learning framework based on coordinate Multi-Layer Perceptron (MLP). The overall workflow framework is displayed in Fig. 1.

3.1. Problem Statement

In this work, we consider the problem of how to improve 3D image registration. Let Ω be a convex bounded open subset of \mathbb{R}^3 (the image spatial domain) of class C^1 thus satisfying the cone property meaning that there exists a finite cone C such that each point $x \in \Omega$ is the vertex of a finite cone C_x contained in Ω and congruent to C , and theoretically required to ensure Ball's results (Ball, 1981). Let $\mathbf{I}_S : \Omega \rightarrow \mathbb{R}$ be the source image to be deformed, and $\mathbf{I}_T : \Omega \rightarrow \mathbb{R}$ be the target image to be fixed. The mapping $\Phi : \bar{\Omega} \rightarrow \mathbb{R}^3$ denotes the sought non-rigid and non-parametric deformation aligning the deformed source image $\mathbf{I}_S(\Phi)$ with the target one \mathbf{I}_T , while $\nabla\Phi : \bar{\Omega} \rightarrow M_3(\mathbb{R})$ is the Jacobian deformation with $M_3(\mathbb{R})$ the set of 3×3 matrices.

Since image registration is highly ill-posed, in an unsupervised deep learning framework in which we place ourselves, the design of the cost function is crucial. Following arguments from the variational setting, the sought deformation is obtained by minimising a loss function comprising two key terms. Firstly, a similarity term that measures how close the deformed source image is to the target image in a sense depending on the application. Secondly, a regularisation term encoding the prescribed nature of the allowed deformations:

$$\hat{\Phi} = \underset{\Phi \in W}{\operatorname{argmin}} \mathcal{L}(\Phi) = \mathcal{L}_{\text{sim}}(\mathbf{I}_S(\Phi), \mathbf{I}_T) + \lambda \mathcal{L}_{\text{reg}}(\Phi), \quad (1)$$

λ is a trade-off parameter between both terms.

3.2. A Novel Conformal-Invariant Regularisation

Inspired by the theory of mechanics, the shapes to be matched are viewed as physical bodies subjected to

forces and undergoing deformations. In this context, a deformation (Ciarlet, 1994) is a smooth mapping that is orientation preserving and injective except possibly on the boundary $\partial\Omega$ if self-contact is allowed which mathematically translates into $\det \nabla \Phi > 0$ almost everywhere. From the variational perspective, it is well-understood that in order to obtain meaningful solutions, one needs to enforce the problem to be well-posed. The key to such is the regulariser.

The majority of learning-based image registration models leverage the empirical properties of a given architecture to approximate the well-posedness of the registration. Whilst they report great performance, they do not provide any guaranteed property yielding to topologically preserving transformations. Motivated by this drawback in the learning-based literature, we introduce a novel regulariser that guarantees homeomorphic transformations—this is translated to have a model that enforces topology preservation yielding to clinically meaningful output. With the previous motivation in mind, our new model falls within the hyperelasticity setting allowing large and non-linear deformations (Ciarlet, 1994, ch. 4) while keeping an elastic behavior and computational performance.

Our motivation to select this principle is that organs and several biological phenomena are characterised by hyperelasticity. We note that highly deformable materials such as rubber, filled elastomer, or biological tissues, are often modelled within this hyperelasticity setting. Unlike linear elasticity assuming small strains and the validity of Hooke's law (linear relation between stress and strains), the hyperelasticity theory predicates the existence of a stored energy density function differentiable with respect to the deformation in each direction and whose derivative gives the state of stress within the material in the same direction. The total deformation stored energy is given by the integral of this density over

the whole body and by minimising this quantity we find a solution to the equilibrium problem (Le Dret, 2003-2004).

In our model, the objects are considered as isotropic (the material deforms in the same way in every direction), homogeneous (meaning that the behavior is the same everywhere inside the material), and hyperelastic materials allowing large compressions and expansions while keeping a mechanical elastic behavior. This interpretation drives the construction of our new regularisation term therefore based on the stored energy of such materials prescribing then a physically-meaningful nature for the generated deformations. Our new regulariser reads:

$$\begin{aligned} \mathcal{L}_{reg}(\Phi) &= \int_{\Omega} W(\nabla\Phi(x), \text{Cof}\nabla\Phi(x), \det\nabla\Phi(x)) dx \\ &+ \mathbf{1}_{\{\|\cdot\|_{L^\infty(\Omega)} \leq \beta\}}(\det\nabla\Phi), \\ \text{with } \beta &> 0, \text{ and } W(\nabla\Phi, \text{Cof}\nabla\Phi, \det\nabla\Phi) = \\ &\left\{ \begin{array}{l} \frac{a_1 \|\nabla\Phi\|_F^9}{(\det\nabla\Phi)^3} + \frac{a_2 \|\text{Cof}\nabla\Phi\|_F^6}{(\det\nabla\Phi)^4} + a_3 (\det\nabla\Phi - 1)^2 + \dots \\ \dots \frac{a_4}{(\det\nabla\Phi)^\alpha} - 3^{\frac{9}{2}} a_1 - 3^{\frac{3}{2}} a_2 - a_4 \text{ if } \det\nabla\Phi > 0 \\ +\infty \text{ otherwise} \end{array} \right. \end{aligned}$$

$\|A\|_F = \sqrt{\text{Tr}(A^T A)}$ being the Frobenius norm, Cof denotes the cofactor matrix, and $\alpha > 1$, $a_1 > 0$, $a_2 > 0$, $a_3 > 0$ and $a_4 > 0$ being hyper-parameters. The first two terms are distortion mappings and measure the deviation from conformality of the deformation and are conformally invariant meaning that any conformal change of variables does not alter their values (Adamowicz, 2007). Our regulariser is then seen as the unification of the hyperelasticity with the conformal and Beltrami-based approaches (Lam and Lui, 2014).

They also control the changes in length and area as well as the smoothness of the deformations. The third and fourth terms are added to control changes in volume that is promoting volume-preserving deformations by penalising deviations from one of the Jacobian determinant while preventing singularities by penalising small values of it. The last constants are added to impose $W(I_3, I_3, 1) = 0$ as required by the hyperelasticity setting. The stored energy density function W is thus poly-convex and rotation-invariant by definition, and the deformations are searched in the following suitable functional space $\mathcal{W} = \{\varphi \in \text{Id} + W_0^{1,9}(\Omega, \mathbb{R}^3) \mid \frac{\|\nabla\varphi\|_F^6}{(\det\nabla\varphi)^3} \in L^1(\Omega), \frac{\|\text{Cof}\nabla\varphi\|_F^6}{(\det\nabla\varphi)^4} \in L^1(\Omega), \det\nabla\varphi \in L^2(\Omega), \frac{1}{\det\nabla\varphi} \in L^\alpha(\Omega), \nabla \det\varphi > 0 \text{ a.e. in } \Omega, \|\det\nabla\varphi\|_{L^\infty(\Omega)} \leq \beta\}$, that is the deformation is assumed to be equal to the identity on the boundary $\partial\Omega$.

Remark 1. This assumption is lifted in practice since the computation of the deformation is done only in the

lung mask inside the image spatial domain Ω as explained in the following section.

Remark 2. The L^∞ penalisation on the Jacobian determinant is added only for theoretical purposes. In practice, β is taken as the maximum value allowed in computers and the penalisation is lifted in the numerical algorithm.

Since $9 > 4$ and

$$\begin{aligned} &\int_{\Omega} \|(\nabla\Phi)^{-1}(x)\|^4 \det\nabla\Phi(x) dx \\ &= \int_{\Omega} \left\| \frac{1}{\det\nabla\Phi(x)} \text{Cof}\nabla\Phi(x)^T \right\|^4 \det\nabla\Phi(x) dx, \\ &= \int_{\Omega} \frac{1}{(\det\nabla\Phi(x))^3} \|\text{Cof}\nabla\Phi(x)\|^4 dx, \\ &= \int_{\Omega} \frac{\|\text{Cof}\nabla\Phi(x)\|^4}{(\det\nabla\Phi(x))^{\frac{8}{3}}} \frac{1}{(\det\nabla\Phi(x))^{\frac{1}{3}}} dx, \\ &\leq \left(\int_{\Omega} \frac{\|\text{Cof}\nabla\Phi(x)\|^6}{(\det\nabla\Phi(x))^4} dx \right)^{\frac{2}{3}} \left(\int_{\Omega} \frac{1}{\det\nabla\Phi(x)} dx \right)^{\frac{1}{3}} \\ &\text{by Holder's inequality with } p = \frac{3}{2} \text{ and } q = 3, \end{aligned} \quad (3)$$

then Ball's results apply (Ball, 1981) and the deformations are homeomorphisms with the inverse deformation $\Phi^{-1} \in W^{1,4}(\Omega, \mathbb{R}^3)$.

Regarding \mathcal{L}_{sim} from (1), in this work, we take the similarity term as the classical normalised cross-correlation between the deformed source image and the target one:

$$\begin{aligned} \mathcal{L}_{sim}(\mathbf{I}_S(\Phi), \mathbf{I}_T) &= -NCC(\mathbf{I}_S(\Phi), \mathbf{I}_T) \\ &= -\frac{\langle \mathbf{I}_S \circ \Phi, \mathbf{I}_T \rangle_{L^2(\Omega)}}{\|\mathbf{I}_S \circ \Phi\|_{L^2(\Omega)} \|\mathbf{I}_T\|_{L^2(\Omega)}} \\ &= -\sum_{p \in \Omega} \frac{(\sum_{p_i \in w} (\mathbf{I}_S(\Phi(p_i)) - \bar{\mathbf{I}}_S(\Phi(p))) (\mathbf{I}_T(p_i) - \bar{\mathbf{I}}_T(p)))^2}{\sum_{p_i \in w} (\mathbf{I}_S(\Phi(p_i)) - \bar{\mathbf{I}}_S(\Phi(p)))^2 \sum_{p_i \in w} (\mathbf{I}_T(p_i) - \bar{\mathbf{I}}_T(p))^2}, \end{aligned}$$

with w being a local window of size n^3 around the current pixel p , and $\bar{\mathbf{I}}_S(\Phi)(p)$ and $\bar{\mathbf{I}}_T(p)$ are the mean intensity of that local window.

3.3. Theoretical results

Theorem 1 (Existence of minimisers). Problem (1) admits at least one minimiser in \mathcal{W} .

Proof 1. The proof follows the arguments of classical direct methods of the calculus of variations. We first

derive a coercivity inequality. Using the fact that $(a - b)^2 \geq \frac{1}{2}a^2 - b^2$, one has :

$$\begin{aligned}\mathcal{L}(\Phi) &\geq \frac{a_1}{\beta^3} \|\nabla\Phi\|_{L^9(\Omega, M_3(\mathbb{R}))}^9 + \frac{a_2}{\beta^4} \|\text{Cof}\nabla\Phi\|_{L^6(\Omega, M_3(\mathbb{R}))}^6 \\ &\quad + \frac{a_3}{2} \|\det\nabla\Phi\|_{L^2(\Omega)}^2 - a_3 \text{meas}(\Omega) + a_4 \|\frac{1}{\det\nabla\Phi}\|_{L^\alpha(\Omega)}^\alpha \\ &\quad - 3^{\frac{9}{2}} a_1 \text{meas}(\Omega) - 3^2 a_2 \text{meas}(\Omega) - a_4 \text{meas}(\Omega) \\ &\quad + \mathbb{1}_{\{\|\cdot\|_{L^\infty(\Omega)} \leq \beta\}}(\det\nabla\Phi),\end{aligned}$$

with meas standing for the measure of the space. The quantity $\mathcal{L}(\Phi)$ is thus bounded below and as for $\Phi = \text{Id}$, the identity map, and suitable β , $\mathcal{L}(\Phi) = -NCC(\mathbf{I}_S, \mathbf{I}_T)$ is finite with \mathbf{I}_S and \mathbf{I}_T continuous. The infimum is thus finite.

Let then $(\Phi_k)_k \in \mathcal{W}$ be a minimising sequence, i.e. $\lim_{k \rightarrow +\infty} \mathcal{L}(\Phi_k) = \inf_{\Phi \in \mathcal{W}} \mathcal{L}(\Phi)$. Hence there exists $K \in \mathbb{N}$ such that $\forall k \in \mathbb{N}, k \geq K$ implies $\mathcal{L}(\Phi_k) \leq \inf_{\Phi \in \mathcal{W}} \mathcal{L}(\Phi) + 1$. From now on, we assume that $k \geq K$. According to the coercivity inequality, one gets :

- (Φ_k) is uniformly bounded according to k in $W^{1,9}(\Omega, \mathbb{R}^3)$ using the generalised Poincaré inequality and the fact that $\Phi = \text{Id}$ on $\partial\Omega$.
- $(\text{Cof}\nabla\Phi_k)$ is uniformly bounded according to k in $L^6(\Omega, M_3(\mathbb{R}))$.
- $(\det\nabla\Phi_k)$ is uniformly bounded according to k in $L^\infty(\Omega)$ and in $L^2(\Omega)$.
- $(\frac{1}{\det\nabla\Phi_k})$ is uniformly bounded according to k in $L^\alpha(\Omega)$.

Thus there exist a subsequence – still denoted by (Φ_k) – and $\bar{\Phi} \in W^{1,9}(\Omega, \mathbb{R}^3)$ such that $\Phi_k \xrightarrow{k \rightarrow +\infty} \bar{\Phi}$ in $W^{1,9}(\Omega, \mathbb{R}^3)$. Moreover, there exists a subsequence (common with the previous one which is always possible) – still denoted by $(\text{Cof}\nabla\Phi_k)$ – and $\gamma \in L^6(\Omega, M_3(\mathbb{R}))$ such that $\text{Cof}\nabla\Phi_k \xrightarrow{k \rightarrow +\infty} \gamma$ in $L^6(\Omega, M_3(\mathbb{R}))$. Furthermore, there exists a subsequence also common with previous ones which is always possible – still denoted by $(\det\nabla\Phi_k)$ – and $\delta \in L^2(\Omega)$ such that $\det\nabla\Phi_k \xrightarrow{k \rightarrow +\infty} \delta$ in $L^2(\Omega)$.

By applying Theorem 8.20 from (Dacorogna, 2008), then $\text{Cof}\nabla\Phi_k \xrightarrow{k \rightarrow +\infty} \text{Cof}\nabla\bar{\Phi}$ in $L^{\frac{9}{2}}(\Omega, M_3(\mathbb{R}))$, and by uniqueness of the weak limit as well as the continuous embedding of L^p -spaces, we have that $\gamma = \text{Cof}\nabla\bar{\Phi}$ in $L^6(\Omega, M_3(\mathbb{R}))$ and thus $\text{Cof}\nabla\Phi_k \xrightarrow{k \rightarrow +\infty} \text{Cof}\nabla\bar{\Phi}$ in $L^6(\Omega, M_3(\mathbb{R}))$. We also get that $\det\nabla\Phi_k \xrightarrow{k \rightarrow +\infty} \det\nabla\bar{\Phi}$ in $L^3(\Omega)$ and by uniqueness of the weak limit as well

as the continuous embedding of L^p -spaces, we get that $\delta = \det\nabla\bar{\Phi}$ in $L^2(\Omega)$ and therefore $\det\nabla\Phi_k \xrightarrow{k \rightarrow +\infty} \det\nabla\bar{\Phi}$ in $L^2(\Omega)$ and $\det\nabla\Phi_k \xrightarrow{k \rightarrow +\infty} \det\bar{\Phi}$ in $L^\infty(\Omega)$. At last, by continuity of the trace operator, we have that $\bar{\Phi} \in \text{Id} + W_0^{1,9}(\Omega, \mathbb{R}^3)$. The stored energy function W is continuous and convex: if $\psi_n \xrightarrow{n \rightarrow +\infty} \bar{\psi}$ in $W^{1,9}(\Omega, \mathbb{R}^3)$, thus $\nabla\psi_n \xrightarrow{n \rightarrow +\infty} \nabla\bar{\psi}$ in $L^9(\Omega, M_3(\mathbb{R}))$ and one can extract a subsequence still denoted by $(\nabla\psi_n)$ such that $\nabla\psi_n \xrightarrow{n \rightarrow +\infty} \nabla\bar{\psi}$ almost everywhere in Ω .

Similarly, if $K_n \xrightarrow{n \rightarrow +\infty} \bar{K}$ in $L^6(\Omega, M_3(\mathbb{R}))$ then one can extract a common subsequence still denoted by (K_n) such that $K_n \xrightarrow{n \rightarrow +\infty} \bar{K}$ almost everywhere in Ω . Finally, if $\delta_n \xrightarrow{n \rightarrow +\infty} \bar{\delta}$ in $L^2(\Omega)$ then one can extract a common subsequence still denoted by (δ_n) such that $\delta_n \xrightarrow{n \rightarrow +\infty} \bar{\delta}$ almost everywhere in Ω . Then, by continuity of W , one gets that $W(\nabla\psi_n, K_n, \delta_n) \xrightarrow{n \rightarrow +\infty} W(\nabla\bar{\psi}, \bar{K}, \bar{\delta})$ almost everywhere in Ω . Then applying Fatou's lemma yields $\int_{\Omega} W(\nabla\bar{\psi}, \bar{K}, \bar{\delta}) dx \leq \liminf_{k \rightarrow +\infty} \int_{\Omega} W(\nabla\psi_n, K_n, \delta_n) dx$. As W is convex, so is $\int_{\Omega} W(\xi, K, \delta) dx$, and involving Brézis Corollaire III.8 (Brezis, 2005) leads to: $\int_{\Omega} W(\nabla\bar{\Phi}, \text{Cof}\nabla\bar{\Phi}, \det\nabla\bar{\Phi}) dx \leq \liminf_{k \rightarrow +\infty} \int_{\Omega} W(\nabla\Phi_k, \text{Cof}\nabla\Phi_k, \det\nabla\Phi_k) dx < +\infty$. Since $W(\nabla\bar{\Phi}, \text{Cof}\nabla\bar{\Phi}, \det\nabla\bar{\Phi}) = +\infty$ when $\det\nabla\bar{\Phi}(x) \leq 0$, the set on which it occurs is necessarily of null measure otherwise we would have $\mathcal{L}(\bar{\Phi}) = +\infty$. So $\det\nabla\bar{\Phi} > 0$ almost everywhere on Ω . Besides, for all $k \geq K$, $\int_{\Omega} \|(\nabla\Phi_k)^{-1}\|_F^4 \det\nabla\Phi_k dx \leq C$. $C = C(\alpha, \beta, \Omega) > 0$ being a constant depending only on α, β and Ω . The assumptions of Ball's results thus hold (Ball, 1981) and it yields that (Φ_k) are homeomorphisms from $\bar{\Omega}$ to $\bar{\Omega}$ and $\Phi_k^{-1} \in W^{1,4}(\Omega, \mathbb{R}^3)$. By the weak-* lower semi-continuity of $\|\cdot\|_{L^\infty(\Omega)}$, we deduce that $\|\det\nabla\bar{\Phi}\|_{L^\infty(\Omega)} \leq \liminf_{k \rightarrow +\infty} \|\det\nabla\Phi_k\|_{L^\infty(\Omega)} \leq \beta$ and $\mathbb{1}_{\{\|\cdot\|_{L^\infty(\Omega)} \leq \beta\}}(\nabla\bar{\Phi}) \leq \liminf_{k \rightarrow +\infty} \mathbb{1}_{\{\|\cdot\|_{L^\infty(\Omega)} \leq \beta\}}(\nabla\Phi_k)$. Also, $\int_{\Omega} \|(\nabla\bar{\Phi})^{-1}\|_F^4 \det\nabla\bar{\Phi} dx < \infty$ following the same calculus as previously. Therefore $\bar{\Phi}$ is also a homeomorphism from $\bar{\Omega}$ to $\bar{\Omega}$. Since $\mathbf{I}_S \in L^2(\Omega) \cap C^0(\Omega)$, we have that $\mathbf{I}_S \circ \Phi_k \xrightarrow{k \rightarrow +\infty} \mathbf{I}_S \circ \bar{\Phi}$ almost everywhere in Ω and thus $NCC(\mathbf{I}_S \circ \Phi_k, \mathbf{I}_R) \xrightarrow{k \rightarrow +\infty} NCC(\mathbf{I}_S \circ \bar{\Phi}, \mathbf{I}_R)$ by using Lebesgue theorem and assuming both \mathbf{I}_S and \mathbf{I}_R are bounded. We thus have proved that $\mathcal{L}(\bar{\Phi}) \leq \liminf_{k \rightarrow +\infty} \mathcal{L}(\Phi_k) = \inf_{\Phi \in \mathcal{W}} \mathcal{L}(\Phi) < +\infty$ with $\bar{\Phi} \in \mathcal{W}$.

3.4. Learning Transformations via Coordinate MLP

In our pair-wise registration framework, we employ a coordinate MLP to continuously represent the transformation. Unlike traditional methods that directly operate on image intensities, we use the spatial coordinates (x, y, z) within the lung area as inputs to the MLP. In our lung CT registration task, due to sophisticated structures in the lungs, we expect that the coordinate MLP can represent high-frequency information, which means local small deformations. To achieve this, we adopt the strategy inspired by SIREN (Sitzmann et al., 2020), which utilizes periodic sinusoidal functions to model high-frequency content effectively. The SIREN strategy is based on the observation that neural networks with sinusoidal activation functions can approximate high-frequency signals more efficiently than traditional activation functions such as ReLU or Sigmoid. By using sinusoidal activations, the network can better represent fine-grained details and capture high-frequency variations.

Take a 3D position $p \in \mathbb{R}^3$ in \mathbf{I}_T as input, set $p' \in \mathbb{R}^3$ as corresponding position in the coordinate space of \mathbf{I}_S . The deformation between p and p' is parameterised as following:

$$\Phi(p) = \sin(\omega(W_i p + b_i)), \quad (4)$$

where ω is the hyperparameter that regulates the spectral bias of the network, we set it as 32 for all our experiments. In our setting, we use a 4-layer MLP for the COPD dataset and a 3-layer MLP for 4DCT dataset with 256 hidden units.

4. Experiments and Results

This section describes in details the range of experiments conducted to evaluate our proposed framework.

4.1. Experimental Setup

In our experimental setup, we introduce the datasets utilised and present our comprehensive implementation details.

4.1.1. Datasets Description

We evaluate our framework on inspiration-to-expiration lung CT registration task using two publicly available dataset: DIRLab COPD (Castillo et al., 2013) and DIRLab 4DCT (Castillo et al., 2009). Both the two datasets are composed of lung CT images characterising the inspiration-to-expiration motion of the lung from 10 patients. They also provide 300 anatomical landmarks

(serve as ground truth for the evaluation) for images that at the inspiration phase and at the expiration phase. More details please refer to the provided website link².

4.1.2. Evaluation Protocol

We follow the standard protocol for evaluating our framework using the target registration error (TRE) as the performance metric. The TRE is defined as the distance between a set of manually identified corresponding points, typically referred to as landmarks, in the registered image and the corresponding points in the target image. In this paper, the 300 corresponding landmarks provided in the dataset are used to calculate the TRE. The lowest the TRE the better the registration output.

4.1.3. Implementation Details.

Our method was implemented using PyTorch, and utilised an NVIDIA A100 GPU for computation. During the training stage, each image pair is trained for 6000 epochs for the COPD dataset, and 3000 epochs for the 4DCT dataset. At each epoch, we randomly sample 15000 points, from the masked image, with only lung information for the COPD dataset (10000 points for the 4DCT dataset). We optimise the network using the Adam optimiser with a fixed learning rate of 1×10^{-5} . The total time required to register one pair of 3D volumes is 1.7 minutes for COPD dataset and 1.1 minutes for the 4DCT dataset. The registration is finished in one-shot without any prior affine registration.

4.2. Experimental Results

For evaluating our proposed method, we compare it against five competitive methods for lung CT registration, which is a challenging task due to the superposition of respiratory and cardiac motion.

4.2.1. Performance Improvement

In Table 1, we report a set of quantitative comparisons in terms of TRE (mm) on the DIRLab COPD dataset between our method and other state-of-the-art methods: 1) FE (Liu et al., 2019b), 2) PDD (Heinrich, 2019), 3) VM (Balakrishnan et al., 2019), 4) LapIRN (Mok and Chung, 2020), and 5) INR (Wolterink et al., 2022). The COPD dataset has extremely large deformation with an average initial displacement of 23.36 mm. The initial TRE of all patients are listed in the second column of

² The dataset is released at the website <https://med.emory.edu/departments/radiation-oncology/research-laboratories/deformable-image-registration/index.html>

Table 1: Numerical comparison of our proposed framework vs. other existing image registration techniques. The numerical values reflect the TRE metric (*mm*) for the DIRLab COPD dataset. The best results are highlighted in green colour.

COPD	<i>Init.</i>	FE	PDD	VM	LapIRN	INR	Ours
01	26.33	4.89	2.57	9.95	6.85	2.53	1.66
02	21.79	7.30	4.01	9.96	6.90	5.78	3.70
03	12.64	2.89	1.46	4.41	1.51	1.28	1.28
04	29.58	5.46	2.19	7.08	6.38	2.34	1.62
05	30.08	5.19	2.22	9.19	6.81	3.09	1.47
06	28.46	5.53	1.89	8.12	4.19	2.66	1.86
07	21.60	4.40	1.62	7.10	2.73	1.27	1.20
08	26.46	3.94	1.72	7.92	4.32	2.75	1.65
09	14.86	3.57	1.51	6.93	3.60	1.40	1.30
10	21.81	4.44	2.43	9.16	6.59	3.25	1.69
<i>Avg.</i>	23.36	4.76	2.16	7.98	4.99	2.64	1.74

Table 2: Numerical comparison of our proposed framework vs. other existing image registration techniques. The numerical values reflect the TRE metric (*mm*) for the DIRLab 4DCT dataset. The best results are highlighted in green colour.

4DCT	<i>Init.</i>	FE	PDD	VM	LapIRN	INR	Ours
01	3.89	2.20	0.90	1.46	1.00	0.76	0.78
02	4.34	3.89	0.91	1.51	1.28	0.76	0.77
03	6.94	2.71	1.06	2.31	2.18	0.94	0.94
04	9.83	2.95	1.66	2.72	3.05	1.32	1.36
05	7.48	3.03	1.68	2.69	2.36	1.23	1.20
06	10.89	3.36	1.86	3.07	1.78	1.09	1.06
07	11.03	3.10	1.94	3.01	2.24	1.12	0.97
08	14.99	2.94	1.79	6.22	2.24	1.21	1.12
09	7.92	2.86	1.94	2.94	2.26	1.22	1.08
10	7.30	2.99	2.03	3.00	1.90	1.01	1.04
<i>Avg.</i>	8.46	3.00	1.57	2.89	2.03	1.07	1.03

the table, denoted as *Init.*. In a closer look at the results, we observe that our method achieved the lowest TRE in all COPD data pairs, with an average value of 1.74 *mm*. We outperform the second-best method INR by 0.42 *mm*. While other methods have much higher average TRE values ranging from 2.16 *mm* to 7.98 *mm*. Similarly, in Table 2, we report TRE results on the 4DCT dataset, our method also achieved the lowest average TRE value compared to other methods, and achieved the lowest TRE value on 6 image pairs.

We also ran a non-parametric test for multiple comparisons using the Friedman test along with Kendall’s coefficient of concordance with 95% confidence intervals as a measure of the effect size for the Friedman test. The statistical analyses for both datasets are reported in Fig. 2. We can conclude that there is a statistically significant difference in performance $\chi^2_{Friedman}(5) = 45.11 \& 46.95$ with $p = 1.38e-08 \& 5.82e-09$. The effect size is $W_{Kendall} = 0.90 \& 0.94$ with 95% CI. We then per-

formed pair-wise comparisons using the non-parametric Wilcoxon test yielding to our technique being statistically significantly different in performance across all compared techniques.

4.2.2. Qualitative Evaluation.

We computed the Jacobian determinant and visually represented the results using a color map, where red indicates a positive determinant and blue indicates a negative determinant. Fig. 3 displays the results of selected patients with: No regularisation, Hyperelastic regularisation (Wolterink et al., 2022; Burger et al., 2013), and our conformal invariant regulariser. We observe that without regularisation, one obtains a large number of negative values for the Jacobian determinant. This indicates that the deformation fields obtained were implausible and resulted in topological distortions. The Hyperelastic regulariser also reports substantial negative values for the Jacobian determinant (blue areas) along with

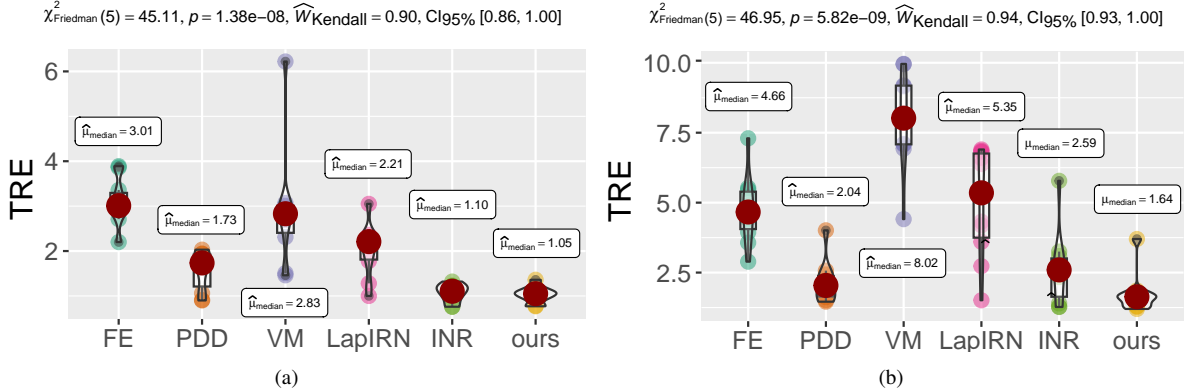


Figure 2: Statistical Analysis of our technique and existing methods. We performed the Friedman test for multiple comparisons along the Wilcoxon test for pair-wise comparison for (a) 4DCT and (b) COPD datasets.

large expansions. In contrast, our regulariser, reported all positive values yielding to clinical meaningful transformations. These findings underscore the importance of appropriate regularisation in image registration and further support the superiority of our proposed registration framework.

4.2.3. Results on Different MLPs.

In this section, we evaluate our conformal invariant regularization by integrating it with different coordinate MLP architectures, specifically MLP with periodic activation function (Wolterink et al., 2022) and Fourier feature mapping MLP (Tancik et al., 2020). The results of both the COPD dataset and the 4DCT dataset are presented in Table 3 and the best results are illustrated in bold font. Results show that MLP with periodic activation achieved the best results. This experiment provides evidence supporting the notion that MLP with a periodic activation function is capable of learning more high-frequency features, thereby capturing finer details in the images.

5. Conclusion and Discussion

It is rather difficult to collect large and representative medical image datasets for training the registration networks. Moreover, existing learning-based registration methods lack theoretical guarantees for ensuring the homeomorphism of the deformation field, a crucial requirement in the medical domain. Therefore, in this paper, we proposed a new homeomorphic registration framework to solve these problems. We explicitly introduced a novel conformal-invariant hyperelastic regularisation, which yields to a clinically meaningful registration. Combining the advantage of neural fields–

Table 3: Numerical comparison between MLP with Periodic Activation Function (‘Periodic’) and MLP with Fourier Feature Mapping (‘Fourier’). The numerical values reflect the TRE metric (mm) for both the DIRLab COPD and the 4DCT datasets. Bold font represents better results.

	COPD		4DCT	
	Periodic	Fourier	Periodic	Fourier
01	1.66	2.11	0.78	0.81
02	3.70	2.46	0.77	0.78
03	1.28	1.56	0.94	1.01
04	1.62	1.88	1.36	1.35
05	1.47	1.87	1.20	1.23
06	1.86	2.52	1.06	1.03
07	1.20	1.61	0.97	1.04
08	1.65	2.16	1.12	1.23
09	1.30	1.72	1.08	1.08
10	1.69	2.35	1.04	1.09
Avg.	1.74	2.02	1.03	1.07

coordinate-based parameterisation of the physical properties across space and time, we build our framework based on a coordinate MLP with a periodic activation function for learning the high-frequency information of the input image pairs. Our extensive experiments on two public lung CT datasets demonstrated the benefits of our registration framework.

One limitation of the proposed work is the computation time required for the registration process. Compared to standard learning-based methods that exhibit rapid inference within a few seconds, our registration framework consumes slightly more time (the total time required to register one pair of 3D volumes is 1.7 minutes for the COPD dataset and 1.1 minutes for the 4DCT

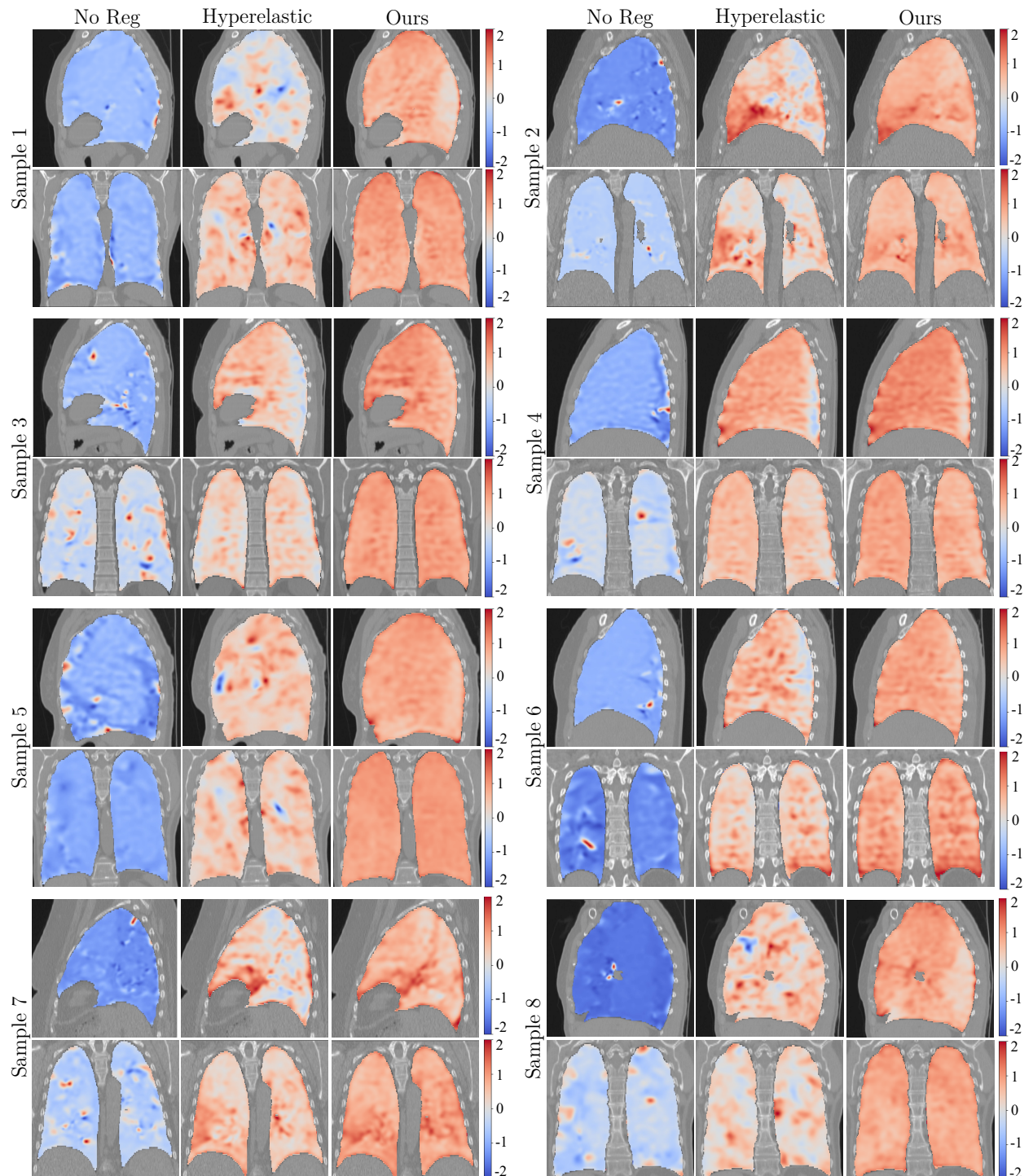


Figure 3: Visual comparison in terms of Jacobian determinant of our proposed regulariser vs. no regularisation ('No Reg') and the most widely used hyperelastic regulariser.

dataset). However, it is important to note that our framework achieves one-shot registration avoiding the training with a large dataset and with no need for pre-affine registration. In this perspective, our registration framework is more computationally efficient. As a consequence, together with the property of homeomorphism, the proposed framework has great potential to be applied in various practical clinical applications, such as tumor tracking in image-guided navigation systems and motion compensation in radiotherapy.

In the future, we plan to investigate mainly two works. Firstly, we will conduct a large cohort evaluation on different organs and modalities to assess the generalizability and robustness of our proposed framework. Secondly, we will explore our regulariser by integrating it with other intensity-based registration networks, we aim to enhance the registration accuracy and robustness even further.

In conclusion, we proposed a novel conformal-invariant hyperelastic regulariser for providing a theoretical guarantee of homeomorphism of the deformation field. To the best of our knowledge, we are the first to achieve homeomorphic registration by combining novel conformal-invariant hyperelastic regulariser with coordinate MLP. In future work, we will conduct more experiments and explore the regulariser in conjunction with other intensity-based networks.

Acknowledgements

Jing Zou and Jing Qin gratefully acknowledge a General Research Fund of Hong Kong Research Grants Council (15205919). Lihao Liu acknowledges the financial support from the GSK Ph.D. Scholarship and the Girton College Graduate Research Award at the University of Cambridge. Angelica I Aviles-Rivero acknowledges the support from the Centre for Mathematical Imaging in Healthcare (CMIH) and the Cantab Capital Institute for the Mathematics of Information (CCIMI) at the University of Cambridge. Carola-Bibiane Schönlieb acknowledges the support from the Philip Leverhulme Prize, the Royal Society Wolfson Fellowship, the EPSRC Advanced Career Fellowship EP/V029428/1, EPSRC grants EP/S026045/1, EP/T003553/1, EP/N014588/1, and EP/T017961/1, the Wellcome Innovator Awards 215733/Z/19/Z and 221633/Z/20/Z, the European Union Horizon 2020 research and innovation programme under the Marie Skłodowska-Curie grant agreement No. 777826 No-MADS, as well as the Cantab Capital Institute for the Mathematics of Information (CCIMI) and the Alan Turing Institute.

References

Adamowicz, T., 2007. The grötzsch problem in higher dimensions. *Rendiconti Lincei-matematica E Applicazioni - REND LINCEI-MAT APPL* 18, 163–177. doi:10.4171/RLM/488.

Ashburner, J., Friston, K.J., 2000. Voxel-based morphometry—the methods. *Neuroimage* 11, 805–821.

Avants, B.B., Epstein, C.L., Grossman, M., Gee, J.C., 2008. Symmetric diffeomorphic image registration with cross-correlation: evaluating automated labeling of elderly and neurodegenerative brain. *Medical image analysis* 12, 26–41.

Avants, B.B., Tustison, N., Song, G., et al., 2009. Advanced normalization tools (ants). *Insight j* 2, 1–35.

Bajcsy, R., Kovačić, S., 1989. Multiresolution elastic matching. *Computer vision, graphics, and image processing* 46, 1–21.

Balakrishnan, G., Zhao, A., Sabuncu, M.R., Guttag, J., Dalca, A.V., 2018. An unsupervised learning model for deformable medical image registration, in: *Proceedings of the IEEE/CVF Conference on Computer Vision and Pattern Recognition*, pp. 9252–9260.

Balakrishnan, G., Zhao, A., Sabuncu, M.R., Guttag, J., Dalca, A.V., 2019. Voxelmorph: a learning framework for deformable medical image registration. *IEEE Transactions on Medical Imaging* 38, 1788–1800.

Ball, J.M., 1981. Global invertibility of Sobolev functions and the interpenetration of matter. *P. Roy. Soc. Edin. A* 88, 315–328.

Beg, M.F., Khan, A., 2007. Symmetric data attachment terms for large deformation image registration. *IEEE transactions on medical imaging* 26, 1179–1189.

Beg, M.F., Miller, M.I., Trouvé, A., Younes, L., 2005. Computing large deformation metric mappings via geodesic flows of diffeomorphisms. *International journal of computer vision* 61, 139–157.

Brezis, H., 2005. *Analyse fonctionnelle*. Dunod Paris.

Brock, K.K., Mutic, S., McNutt, T.R., Li, H., Kessler, M.L., 2017. Use of image registration and fusion algorithms and techniques in radiotherapy: Report of the aapm radiation therapy committee task group no. 132. *Medical physics* 44, e43–e76.

Burger, M., Modersitzki, J., Rutherford, L., 2013. A hyperelastic regularization energy for image registration. *SIAM Journal on Scientific Computing* 35, B132–B148.

Cao, Y., Miller, M.I., Winslow, R.L., Younes, L., 2005. Large deformation diffeomorphic metric mapping of vector fields. *IEEE transactions on medical imaging* 24, 1216–1230.

Castillo, R., Castillo, E., Fuentes, D., Ahmad, M., Wood, A.M., Ludwig, M.S., Guerrero, T., 2013. A reference dataset for deformable image registration spatial accuracy evaluation using the copdgene study archive. *Physics in Medicine & Biology* 58, 2861.

Castillo, R., Castillo, E., Guerra, R., Johnson, V.E., McPhail, T., Garg, A.K., Guerrero, T., 2009. A framework for evaluation of deformable image registration spatial accuracy using large landmark point sets. *Physics in Medicine & Biology* 54, 1849.

Christensen, G.E., Rabbitt, R.D., Miller, M.I., 1996. Deformable templates using large deformation kinematics. *IEEE Transactions on Image Processing* 5, 1435–1447.

Ciarlet, P., 1994. *Three-Dimensional Elasticity. Mathematical Elasticity*. Elsevier Science.

Çiçek, Ö., Abdulkadir, A., Lienkamp, S.S., Brox, T., Ronneberger, O., 2016. 3d u-net: learning dense volumetric segmentation from sparse annotation, in: *International Conference on Medical Image Computing and Computer-Assisted Intervention*, Springer. pp. 424–432.

Dacorogna, B., 2008. *Direct Methods in the Calculus of Variations, Second Edition*. Springer.

De Vos, B.D., Berendsen, F.F., Viergever, M.A., Sokooti, H., Staring, M., Işgum, I., 2019. A deep learning framework for unsupervised

affine and deformable image registration. *Medical image analysis* 52, 128–143.

Fan, J., Cao, X., Yap, P.T., Shen, D., 2019. Birnet: Brain image registration using dual-supervised fully convolutional networks. *Medical image analysis* 54, 193–206.

Glaunès, J., Qiu, A., Miller, M.J., Younes, L., 2008. Large deformation diffeomorphic metric curve mapping. *International journal of computer vision* 80, 317–336.

Han, K., Sun, S., Yan, X., You, C., Tang, H., Naushad, J., Ma, H., Kong, D., Xie, X., 2023. Diffeomorphic image registration with neural velocity field, in: *Proceedings of the IEEE/CVF Winter Conference on Applications of Computer Vision*, pp. 1869–1879.

Heinrich, M.P., 2019. Closing the gap between deep and conventional image registration using probabilistic dense displacement networks, in: *International Conference on Medical Image Computing and Computer-Assisted Intervention*, Springer. pp. 50–58.

Hering, A., Häger, S., Moltz, J., Lessmann, N., Heldmann, S., van Ginneken, B., 2021. CNN-based lung CT registration with multiple anatomical constraints. *Medical Image Analysis* 72, 102139.

Kim, B., Kim, D.H., Park, S.H., Kim, J., Lee, J.G., Ye, J.C., 2021. Cyclemorph: cycle consistent unsupervised deformable image registration. *Medical Image Analysis* 71, 102036.

Kim, B., Kim, J., Lee, J.G., Kim, D.H., Park, S.H., Ye, J.C., 2019. Unsupervised deformable image registration using cycle-consistent cnn, in: *International Conference on Medical Image Computing and Computer-Assisted Intervention*, Springer. pp. 166–174.

Klein, S., Staring, M., Murphy, K., Viergever, M.A., Pluim, J.P., 2009. Elastix: a toolbox for intensity-based medical image registration. *IEEE transactions on medical imaging* 29, 196–205.

Krilavicius, T., Zliobaite, I., Simonavicius, H., Jaruevicius, L., 2016. Predicting respiratory motion for real-time tumour tracking in radiotherapy, in: *International Symposium on Computer-Based Medical Systems (CBMS)*, IEEE. pp. 7–12.

Lam, K.C., Lui, L.M., 2014. Landmark- and intensity-based registration with large deformations via quasi-conformal maps. *SIAM Journal on Imaging Sciences* 7, 2364–2392. doi:10.1137/130943406.

Le Dret, H., 2003-2004. Notes de Cours de DEA. Méthodes mathématiques en élasticité.

Liu, J., Aviles-Rivero, A.I., Ji, H., Schönlieb, C.B., 2021. Rethinking medical image reconstruction via shape prior, going deeper and faster: Deep joint indirect registration and reconstruction. *Medical Image Analysis* 68, 101930.

Liu, L., Hu, X., Zhu, L., Heng, P.A., 2019a. Probabilistic multilayer regularization network for unsupervised 3D brain image registration, in: *International Conference on Medical Image Computing and Computer-Assisted Intervention*, Springer. pp. 346–354.

Liu, L., Huang, Z., Liò, P., Schönlieb, C.B., Aviles-Rivero, A.I., 2022. Pe-swinmorph: patch representation for unsupervised medical image registration and segmentation. *arXiv preprint arXiv:2203.05684*.

Liu, X., Qi, C.R., Guibas, L.J., 2019b. Flownet3d: Learning scene flow in 3D point clouds, in: *Proceedings of the IEEE/CVF Conference on Computer Vision and Pattern Recognition*, pp. 529–537.

Long, J., Shelhamer, E., Darrell, T., 2015. Fully convolutional networks for semantic segmentation, in: *Proceedings of the IEEE Conference on Computer Vision and Pattern Recognition*, pp. 3431–3440.

Mansi, T., Pennec, X., Sermesant, M., Delingette, H., Ayache, N., 2011. ilogdemons: A demons-based registration algorithm for tracking incompressible elastic biological tissues. *International Journal of Computer Vision* 92, 92–111.

Modersitzki, J., 2003. Numerical methods for image registration. OUP Oxford.

Mok, T.C., Chung, A.C., 2020. Large deformation diffeomorphic image registration with laplacian pyramid networks, in: *International Conference on Medical Image Computing and Computer-Assisted Intervention*, Springer. pp. 211–221.

Oliveira, F.P., Tavares, J.M.R., 2014. Medical image registration: a review. *Computer methods in biomechanics and biomedical engineering* 17, 73–93.

Passieux, J.C., Périé, J.N., 2012. High resolution digital image correlation using proper generalized decomposition: Pgd-dic. *International Journal for Numerical Methods in Engineering* 92, 531–550.

Pennec, X., Cachier, P., Ayache, N., 1999. Understanding the “demon’s algorithm”: 3d non-rigid registration by gradient descent, in: *Medical Image Computing and Computer-Assisted Intervention—MICCAI’99: Second International Conference*, Cambridge, UK, September 19–22, 1999. Proceedings 2, Springer. pp. 597–605.

Phatak, N.S., Maas, S.A., Veress, A.I., Pack, N.A., Di Bella, E.V., Weiss, J.A., 2009. Strain measurement in the left ventricle during systole with deformable image registration. *Medical Image Analysis* 13, 354–361.

Rogelj, P., Kovačič, S., 2006. Symmetric image registration. *Medical image analysis* 10, 484–493.

Ronneberger, O., Fischer, P., Brox, T., 2015. U-net: Convolutional networks for biomedical image segmentation, in: *International Conference on Medical Image Computing and Computer-Assisted Intervention*, Springer. pp. 234–241.

Rueckert, D., Sonoda, L.I., Hayes, C., Hill, D.L., Leach, M.O., Hawkes, D.J., 1999. Nonrigid registration using free-form deformations: application to breast mr images. *IEEE Transactions on Medical Imaging* 18, 712–721.

Sitzmann, V., Martel, J., Bergman, A., Lindell, D., Wetzstein, G., 2020. Implicit neural representations with periodic activation functions. *Advances in Neural Information Processing Systems* 33, 7462–7473.

Sokooti, H., de Vos, B., Berendsen, F., Ghafoorian, M., Yousefi, S., Lelieveldt, B.P., Isgum, I., Staring, M., 2019. 3d convolutional neural networks image registration based on efficient supervised learning from artificial deformations. *arXiv preprint arXiv:1908.10235*.

Sokooti, H., Vos, B.d., Berendsen, F., Lelieveldt, B.P., Isgum, I., Staring, M., 2017. Nonrigid image registration using multi-scale 3d convolutional neural networks, in: *International conference on medical image computing and computer-assisted intervention*, Springer. pp. 232–239.

Tam, A.L., Lim, H.J., Wistuba, I.I., Tamrazi, A., Kuo, M.D., Ziv, E., Wong, S., Shih, A.J., et al., 2016. Image-guided biopsy in the era of personalized cancer care: proceedings from the society of interventional radiology research consensus panel. *Journal of Vascular and Interventional Radiology: JVIR* 27, 8.

Tancik, M., Srinivasan, P., Mildenhall, B., Fridovich-Keil, S., Raghavan, N., Singhal, U., Ramamoorthi, R., Barron, J., Ng, R., 2020. Fourier features let networks learn high frequency functions in low dimensional domains. *Advances in Neural Information Processing Systems* 33, 7537–7547.

Tekchandani, H., Verma, S., Londhe, N.D., Jain, R.R., Tiwari, A., 2022. Computer aided diagnosis system for cervical lymph nodes in CT images using deep learning. *Biomedical Signal Processing and Control* 71, 103158.

Vercauteren, T., Pennec, X., Perchant, A., Ayache, N., 2009. Diffeomorphic demons: Efficient non-parametric image registration. *NeuroImage* 45, S61–S72.

Veress, A.I., Gullberg, G.T., Weiss, J.A., 2005. Measurement of strain in the left ventricle during diastole with cine-MRI and deformable image registration. *J Biomech Eng*.

Vialard, F.X., Risser, L., Rueckert, D., Cotter, C.J., 2012. Diffeomorphic 3d image registration via geodesic shooting using an efficient

adjoint calculation. *International Journal of Computer Vision* 97, 229–241.

Wolterink, J.M., Zwienenberg, J.C., Brune, C., 2022. Implicit neural representations for deformable image registration, in: International Conference on Medical Imaging with Deep Learning, PMLR. pp. 1349–1359.

Xu, Z., Niethammer, M., 2019. Deepatlas: Joint semi-supervised learning of image registration and segmentation, in: International Conference on Medical Image Computing and Computer-Assisted Intervention, Springer. pp. 420–429.

Yang, X., Kwitt, R., Styner, M., Niethammer, M., 2017. Fast predictive multimodal image registration, in: 2017 IEEE 14th International Symposium on Biomedical Imaging (ISBI 2017), IEEE. pp. 858–862.

Zhao, S., Dong, Y., Chang, E.J., Xu, Y., et al., 2019a. Recursive cascaded networks for unsupervised medical image registration, in: Proceedings of the IEEE/CVF International Conference on Computer Vision, pp. 10600–10610.

Zhao, S., Lau, T., Luo, J., Eric, I., Chang, C., Xu, Y., 2019b. Unsupervised 3d end-to-end medical image registration with volume tweening network. *IEEE journal of biomedical and health informatics* 24, 1394–1404.

Zhu, Y., Lu, S., 2022. Swin-voxelmorph: A symmetric unsupervised learning model for deformable medical image registration using swin transformer, in: International Conference on Medical Image Computing and Computer-Assisted Intervention., Springer. pp. 78–87.

Zou, J., Liu, L., Song, Y., Choi, K.S., Qin, J., 2022. Deformable lung CT registration by decomposing large deformation, in: Biomedical Image Registration: 10th International Workshop, WBIR 2022, Munich, Germany, July 10–12, 2022, Proceedings, Springer. pp. 185–189.